EUROFUSION WPCD-PR(15) 14804

S. Sesnic et al.

A Finite Element versus Analytical Approach to the Solution of the Current Diffusion Equation in Tokamaks

Preprint of Paper to be submitted for publication in
IEEE Transactions on Plasma Science

This work has been carried out within the framework of the EUROfusion Consortium and has received funding from the Euratom research and training programme 2014-2018 under grant agreement No 633053. The views and opinions expressed herein do not necessarily reflect those of the European Commission.

A Finite Element versus Analytical Approach to the Solution of the Current Diffusion Equation in Tokamaks

S. Šesnić,[1,a,b] V. Dorić,[2,b] D. Poljak,[2,b] A. Šušnjara,[2,b] J.-F. Artaud[3,b] and J. Urban[4,b]

[1]*Department of Power Engineering, University of Split, Split, 21000, Croatia*

[2]*Department of Electronics, University of Split, Split, 21000, Croatia*

[3]*CEA, IRFM, F-13108 Saint Paul Lez Durance, France*

[4]*Institute of Plasma Physics AS CR, Za Slovankou 3, 182 00 Prague 8, Czech Republic*

[a] Electronic mail: silvestar.sesnic@fesb.hr

[b] All of the authors contributed equally to this work.

The paper presents two new approaches for solving the Current Diffusion Equation (CDE) which governs current diffusion through the conductive plasma inside a tokamak and compares them to CRONOS tokamak simulation suite, as well. Namely, CDE is solved via Finite Element Method (FEM) and analytical technique, respectively, and the obtained results are subsequently compared with the solution obtained from the state-of-the-art CRONOS suite with finite difference calculations. The FEM solution is carried out featuring the use of linear and Hermite type shape functions, respectively, while the analytical solution is obtained by applying certain approximations to the CDE. The trade-off between different approaches has been undertaken. Thus, the results obtained via FEM approach (with Hermite basis function, in particular) show very good agreement with the CRONOS results, while also providing the stability of the solution. On the other hand, the results obtained via the analytical solution clearly demonstrate a good agreement with the numerical results in the edge region, which makes it very useful for various applications, e.g. for benchmarking purposes.

Contents

I. INTRODUCTION

Given the complexity of phenomena occurring in tokamak plasma, an integrated approach is often adopted for simulating the global behavior of a tokamak discharge [1]. In particular, taking into account the axisymmetry of a tokamak and relevant temporal and spatial scales orderings, time evolution equations for the transport of macroscopic plasma quantities, such as current density, pressure, density, etc., can be casted in time and a single space coordinate. The space coordinate arises from flux surface averaging, which is possible due to the much faster transport along the magnetic field lines compared to the perpendicular transport. Typically, this coordinate is the (normalized) toroidal magnetic flux. The flux surface topology is determined by the MHD equilibrium, described by the Grad-Shafranov equation (GSE) [2]. Rigorous derivation of the transport equations, which starts from the kinetic description and involves gyromotion averaging, fluid and MHD equations and flux surface averaging, is reviewed in [3].

The so-called Current Diffusion Equation (CDE) describes the current (or, equivalently, the magnetic field) diffusion through the plasma as a conductive medium. CDE is derived by flux-averaging the Ohm's law. It is this transport equation that is most tightly coupled with the equilibrium (the Grad-Shafranov equation). In view of improving this coupling by employing higher-order numerical schemes, this present paper assesses Finite Element Method (FEM) using Hermite basis functions and an analytical solution of CDE. The results obtained via different approaches agree satisfactorily.

II. CURRENT DIFFUSION AND EQUILIBRIUM IN TOKAMAKS

The evolution of the magnetic field configuration in axisymmetric tokamak devices can be described by a coupled system of the so-called Current Diffusion Equation (CDE) and the

Grad-Shafranov equation (GSE) [4]. The coupling considered here is the adiabatic evolution of the equilibrium, which is a so-called generalized (or queer) differential equation problem, as described by Grad, Hogan et al. [5, 6]. The Grad-Shafranov equation follows from the radial force equilibrium of the tokamak and the magnetic field geometry:

$$R\frac{\partial}{\partial R}\frac{1}{R}\frac{\partial \psi}{\partial R}+\frac{\partial^2 \psi}{\partial Z^2}=-\mu_0 R j_\phi=-\mu_0 R^2\frac{\mathrm{d}p}{\mathrm{d}\psi}-\frac{1}{\mu_0}F\frac{\mathrm{d}F}{\mathrm{d}\psi} \tag{1}$$

where $\psi(R,Z)$ is the poloidal magnetic flux per radian, $j_\phi(R,Z)$ is the toroidal current density, $p(\psi)$ is the plasma pressure, $F(\psi)=RB_\phi$ is the diamagnetic function, $\mathbf{B}=(B_R,B_\phi,B_Z)$ is the magnetic field, μ_0 is the vacuum permeability and (R,ϕ,Z) are toroidal coordinates, as shown in **FIG. 1.** .

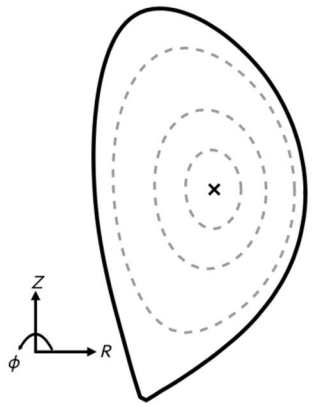

FIG. 1. The toroidally symmetric geometry of a tokamak plasma in a poloidal cut. The solid bold line depicts the plasma boundary (the last closed magnetic surface), dashed lines represent several flux surfaces, on which the magnetic flux is constant. The magnetic axis position is marked by the cross.

The current diffusion equation is derived by flux-averaging the parallel Ohm's law and can be casted in the following form [7]:

$$\begin{aligned}&\frac{\partial \psi}{\partial t}-\frac{\left\langle |\nabla\rho|^2/R^2\right\rangle}{\mu_0\sigma_\parallel\rho_1^2\left\langle 1/R^2\right\rangle}\frac{\partial^2\psi}{\partial x^2}\\&-\left[\frac{\left\langle |\nabla\rho|^2/R^2\right\rangle}{\mu_0\sigma_\parallel\rho_1^2\left\langle 1/R^2\right\rangle}\frac{\partial}{\partial x}\ln\left(\frac{V'\left\langle |\nabla\rho|^2/R^2\right\rangle}{F}\right)+\frac{x}{\rho_1}\frac{d\rho_1}{dt}+\frac{x}{2B_0}\frac{dB_0}{dt}\right]\frac{\partial\psi}{\partial x}=\frac{B_0}{\sigma_\parallel F\left\langle 1/R^2\right\rangle}j_{\mathrm{ni}}\end{aligned} \tag{2}$$

Here, Φ is the toroidal magnetic flux, B_0 the vacuum magnetic field at a given R_0, $\sigma_{\|}$ the parallel conductivity, V the plasma volume enclosed by a flux surface, $V' = \mathrm{d}V/\mathrm{d}\rho$ and j_{ni} is the non-inductive current density. The flux coordinate $x = \rho/\rho_1$, $\rho = \sqrt{\Phi/\pi B_0}$ with ρ_1 its value at the plasma boundary (the last closed flux surface) and Φ the toroidal magnetic field flux in a given flux surface. The flux surface averaging operator is defined as $\langle A \rangle \equiv \partial/\partial V \int_V A \mathrm{d}V$ [8].

The following substitutions can be introduced

$$\left\langle 1/R^2 \right\rangle = g_1 \tag{3}$$

$$\left\langle |\nabla\rho|^2 / R^2 \right\rangle = g_2 \tag{4}$$

and expression (2) becomes

$$\frac{\partial\psi}{\partial t} - \frac{g_2}{\mu_0\sigma_{\|}\rho_1^2 g_1}\frac{\partial^2\psi}{\partial x^2} - \left[\frac{g_2}{\mu_0\sigma_{\|}\rho_1^2 g_1}\frac{\partial}{\partial x}\ln\left(\frac{V'g_2}{F}\right) + \frac{x}{\rho_1}\frac{d\rho_1}{dt} + \frac{x}{2B_0}\frac{dB_0}{dt}\right]\frac{\partial\psi}{\partial x} = \frac{B_0}{\sigma_{\|}Fg_1} j_{ni} \tag{5}$$

A. Coupling of current diffusion and equilibrium

In the Grad-Hogan coupling scheme [6], which is considered in this paper as well as in CRONOS [7] and ASTRA [9] transport suites or in the European Transport Simulator (ETS) [10], the current diffusion (as well as other transport equations) is advanced in time using the geometry from the last GSE solution. GSE is then solved using the resulting $p'(\bar{\psi})$ and $FF'(\bar{\psi})$ profiles. The two equations are iterated until they yield consistent results in terms of the magnetic flux and the plasma current profiles. Here, $\bar{\psi} = (\psi - \psi_0)/(\psi_1 - \psi_0)$ is the normalized poloidal flux with $\bar{\psi} = 0$ on the magnetic axis and $\bar{\psi} = 1$ on the plasma boundary. While p' can be calculated directly from the transport equations results, FF' must be solved for using the averaged Grad-Shafranov equation (AGSE):

$$FF' = \frac{\mu_0}{g_1}\left(\left\langle \frac{j_\phi}{R} \right\rangle - p'\right) \tag{6}$$

The average current term can be calculated as

$$\left\langle j_\phi / R \right\rangle = -\frac{\dfrac{\partial}{\partial x}\left(V' g_2 \dfrac{\partial \psi}{\partial x} \right)}{\rho_1^2 \mu_0 V'} \tag{7}$$

Since the current density must be continuous, it follows that

$$\psi \in C^2, g_2 \in C^1, V' \in C^1 \tag{8}$$

The iteration between CDE and GSE via AGSE is prone to numerical instabilities, as discussed recently in [9] and the references therein. It is thus of great importance to employ a stable, high-accuracy numerical solver for the diffusion equation(s) that inherently yields smooth solutions.

B. Boundary conditions

On the magnetic axis, the geometry of the problem yields

$$\left.\frac{\partial \psi}{\partial x}\right|_{x=0} = 0 . \tag{9}$$

The most common boundary condition on the plasma boundary is related to a prescribed total plasma current (see e.g. [4])

$$I_\mathrm{p} = -\frac{1}{2\pi\mu_0} V' g_2 \left.\frac{\partial \psi}{\partial \rho}\right|_{x=1} \tag{10}$$

However, if the plasma current is not prescribed, we have to consider a different boundary condition. This is often the case with free boundary equilibrium (FBE) simulations. As the magnetic flux is required to be consistent in the transport and equilibrium equations, the natural boundary condition at the last closed flux surface ($x = 1$) would be defined by the equality of the boundary magnetic flux, i.e.

$$\psi^{\mathrm{diff}} = \psi^{\mathrm{equi}} \tag{11}$$

where ψ^{diff} and ψ^{equi} come, respectively, from the solutions of the current diffusion equation and the equilibrium equation. This is similar to prescribing the loop voltage in fixed boundary simulation, which is known to be prone to numerical errors. For this reason, we can use an plasma current predictor I_p^*, derived from (11) using $L_\mathrm{i} I_\mathrm{p} = \psi_0 - \psi_1$. Here, the subscripts 0 and 1 denote the values on the magnetic axis ($x = 0$) and the plasma boundary ($x = 1$) and L_i is the internal inductance of the plasma. Then

$$I_{\mathrm{p}}^{*} = I_{\mathrm{p}}\left(1+\frac{\psi_1^{\mathrm{diff}}-\psi_1^{\mathrm{equi}}}{\psi_0^{\mathrm{equi}}-\psi_1^{\mathrm{equi}}}\right). \tag{12}$$

III. FINITE ELEMENT SOLUTION METHOD

If it can be assumed that $\mathrm{d}B_0/\mathrm{d}t = 0$, as it is defined in [11], the current diffusion equation (5) can be written in the following form

$$\mu_0\sigma_{\|}\rho_1^2\frac{g_1}{g_2}\frac{\partial\psi}{\partial t} = \frac{\partial^2\psi}{\partial x^2}+\left[\frac{\partial}{\partial x}\ln\left(\frac{V'g_2}{F}\right)+\mu_0\sigma_{\|}\rho_1 x\frac{d\rho_1}{dt}\frac{g_1}{g_2}\right]\frac{\partial\psi}{\partial x}+\frac{\mu_0 B_0\rho_1^2}{Fg_2}j_{ni}. \tag{13}$$

The derivation of the *ln* term is carried out analytically

$$\frac{\partial}{\partial x}\ln\left(\frac{V'g_2}{F}\right) = \frac{V''g_2F+V'g_2'F-V'g_2F'}{V'g_2F} \equiv LN(x). \tag{14}$$

Taking the scalar product of CDE with test functions W_j over the calculation domain is yields

$$\begin{aligned}&\mu_0\rho_1^2\int_0^1\sigma\frac{g_1}{g_2}\frac{\partial\psi}{\partial t}W_j dx\\ &=\int_0^1\frac{\partial^2\psi}{\partial x^2}W_j dx+\int_0^1\left[LN(x)+\mu_0\sigma\rho_1 x\frac{d\rho_1}{dt}\frac{g_1}{g_2}\right]\frac{\partial\psi}{\partial x}W_j dx+\int_0^1\frac{\mu_0 B_0\rho_1^2}{Fg_2}j_{ni}W_j dx\end{aligned}. \tag{15}$$

In order to avoid the second order differentiation of the unknown function, the integration by parts is applied to the first term on the right hand side

$$\int_0^1\frac{\partial^2\psi}{\partial x^2}W_j dx = \frac{\partial\psi}{\partial x}W_j\Big|_{x=0}^{x=1}-\int_0^1\frac{\partial\psi}{\partial x}\frac{\partial W_j}{\partial x}dx \tag{16}$$

Term $\frac{\partial\psi}{\partial x}W_j\Big|_{x=0}^{x=1}$ represents the Neumman boundary conditions given with (9) and (10) and can be directly included into matrix equation.

Than the weak form of the current diffusion equation can be written as follows

$$\begin{aligned}&\mu_0\rho_1^2\int\sigma\frac{g_1}{g_2}\frac{\partial\psi}{\partial t}W_j dx\\ &=-\int\frac{\partial\psi}{\partial x}\frac{\partial W_j}{\partial x}dx+\int\left[LN(x)+\mu_0\sigma\rho_1 x\frac{d\rho_1}{dt}\frac{g_1}{g_2}\right]\frac{\partial\Psi}{\partial x}W_j dx+\mu_0 B_0\rho_1^2\int\frac{j_{ni}}{Fg_2}W_j dx\end{aligned}. \tag{17}$$

According to the standard finite element procedure, the unknown magnetic flux ψ is expressed in terms of linearly independent basis functions $\{N_i\}$ with unknown complex coefficients ψ_i, i.e.

$$\psi = \sum_i \psi_i(t) N_i(x). \tag{18}$$

Choosing the same basis functions as test functions $W_j = N_j$ the Gallerkin-Bubnov procedure is introduced to the weak formulation of the current diffusion equation

$$\begin{aligned}
&\mu_0 \rho_1^2 \sum_i \int_0^1 \sigma \frac{g_1}{g_2} N_i N_j dx \cdot \frac{\partial \psi_i}{\partial t} \\
&= \sum_i \left\{ \int_0^1 \left[LN(x) + \mu_0 \sigma \rho_1 x \frac{d\rho_1}{dt} \frac{g_1}{g_2} \right] \frac{\partial N_i}{\partial x} N_j dx - \int_0^1 \frac{\partial N_i}{\partial x} \frac{\partial N_j}{\partial x} dx \right\} \psi_i , \\
&+ \mu_0 B_0 \rho_1^2 \int_0^1 \frac{j_{ni}}{F g_2} N_j dx, \; j = 1, 2, ..., n
\end{aligned} \tag{19}$$

which can, for the sake of simplicity, be written in the form of matrix equation

$$M \frac{\partial \psi}{\partial t} = D\psi + K , \tag{20}$$

Where

$$M = \mu_0 \rho_1^2 \int_0^1 \sigma \frac{g_1}{g_2} N_i N_j dx \tag{21}$$

$$D = -\int_0^1 \frac{\partial N_i}{\partial x} \frac{\partial N_j}{\partial x} dx + \int_0^1 \left[LN(x) + \mu_0 \sigma \rho_1 x \frac{d\rho_1}{dt} \frac{g_1}{g_2} \right] \frac{\partial N_i}{\partial x} N_j dx \tag{22}$$

$$K = \mu_0 B_0 \rho_1^2 \int_0^1 \frac{j_{ni}}{F g_2} N_j dx \tag{23}$$

According to the time domain discretization procedure [9], the solution for the magnetic flux at n+1 time instant is calculated using the solution for the n-th time instant given with

$$\left(M - \Delta t D\right) \psi_{n+1} = M \psi_n + \Delta t K . \tag{24}$$

A. Linear shape functions

Linear shape functions chosen for the basis functions are given with

$$N_1^e = \frac{x_2^e - x}{x_2^e - x_1^e}; \quad N_2^e = \frac{x - x_1^e}{x_2^e - x_1^e} \tag{25}$$

and matrices *M*, *D* and vector *K*, according to finite elements procedure, are assembled from the local matrices as follows

$$\left[M\right]^{e_k} = \mu_0 \rho_1^2 \int_{x_k}^{x_{k+1}} \sigma \frac{g_1}{g_2} N_i^e N_j^e dx \tag{26}$$

$$\left[D\right]^{e_k} = -\int_{x_k}^{x_{k+1}} \frac{\partial N_i^e}{\partial x} \frac{\partial N_j^e}{\partial x} dx + \int_{x_k}^{x_{k+1}} \left[LN(x) + \mu_0 \sigma \rho_1 x \frac{d\rho_1}{dt} \frac{g_1}{g_2} \right] \frac{\partial N_i^e}{\partial x} N_j^e dx \tag{27}$$

$$\left[K\right]^{e_k} = \mu_0 B_0 \rho_1^2 \int_{x_k}^{x_{k+1}} \frac{j_{ni}}{F g_2} N_j^e dx \tag{28}$$

Integrals in (26), (27) and (28) are calculated using the Gaussian four point quadrature rule. The values of the coefficients g_1, g_2, F, V' at the Gaussian points over the element are obtained using linear interpolation. First and second derivative of the resulting poloidal flux are obtained using the smooth noise-robust differentiators described in [12].

B. Hermite shape functions

Hermite interpolation on [-1;1] involves choosing a set of ordered nodes $x_1, ..., x_n \in [-1;1]$ and approximating a smooth function $f(x)$ using its values and derivatives on the nodal set

$$p(x) = \sum_{k=1}^{n} f(x_k) l_k^0(x) + f'(x_k) l_k^1(x), \tag{29}$$

where l_k^0 and l_k^1 are the Hermite interpolating polynomials and they satisfy conditions

$$l_k^0(x_j) = \delta_{jk}, \quad \frac{dl_k^0}{dx}(x_j) = \delta_{jk}, \quad l_k^1(x_j) = 0 \quad \frac{dl_k^1}{dx}(x_j) = 0. \tag{30}$$

After solving the equation (19) with Hermite shape functions, the results comprise both poloidal flux and its first derivative. The second derivative is obtained using smooth robust differentiators [12].

IV. ANALYTICAL SOLUTION PROCEDURE

In order to obtain fundamental analytical solution of (5), time derivative of ρ_1 is neglected and current density driven by non-inductive sources is equal to zero. Taking this into account (5) becomes

$$\frac{\partial \psi}{\partial t} - \frac{g_2}{\mu_0 \sigma_{\|} \rho_1^2 g_1} \frac{\partial^2 \psi}{\partial x^2} - \left[\frac{g_2}{\mu_0 \sigma_{\|} \rho_1^2 g_1} \frac{\partial}{\partial x} \ln\left(\frac{V' g_2}{F} \right) \right] \frac{\partial \psi}{\partial x} = 0 . \tag{31}$$

If following expressions are introduced

$$f(x) = \frac{g_2}{\mu_0 \sigma_{\|} \rho_1^2 g_1}, \tag{32}$$

$$g(x) = \frac{g_2}{\mu_0 \sigma_{\|} \rho_1^2 g_1} \frac{\partial}{\partial x} \ln\left(\frac{V' g_2}{F} \right) \tag{33}$$

equation (31) can be written as

$$\frac{\partial \psi}{\partial t} - f(x) \frac{\partial^2 \psi}{\partial x^2} - g(x) \frac{\partial \psi}{\partial x} = 0 . \tag{34}$$

The particular solution of (34) can be obtained in the form [13]

$$\psi(x,t) = At\Phi(x) + A \int F(x) \int \frac{\Phi(x)\,dx}{f(x) F(x)} dx , \tag{35}$$

where A is an arbitrary constant and auxiliary functions $F(x)$ and $\Phi(x)$ are given with

$$\begin{aligned} F(x) &= \exp\left(-\int \frac{g(x)}{f(x)} dx \right) . \\ \Phi(x) &= \int F(x)\,dx \end{aligned} \tag{36}$$

Undertaking additional mathematical manipulation, the expression for the space-time dependent poloidal flux is obtained

$$\psi(x,t) = At \int \frac{F}{V' g_2} dx + A \mu_0 \rho_1^2 \int\int \frac{\sigma_{\|} g_1 V'}{F} \int \frac{F}{V' g_2} dx dx dx , \tag{37}$$

where arbitrary constant A is calculated from the boundary condition

$$\left. \frac{\partial \psi}{\partial x} \right|_{x=1} = -\left(\frac{2\pi \mu_0 \rho_1}{V' g_2} I_P \right)_{x=1} \tag{38}$$

and is given with

$$A = -\frac{2\pi}{\rho_1 \int \frac{F}{V' g_2} \int \frac{\sigma_{\|} g_1 V'}{F} dxdx} I_p . \tag{39}$$

The functions that appear under the integral (F, V', g_1, g_2) are obtained as an input in the form of discrete data sets which are transformed into polynomial of arbitrary order in a least squares sense.

The first derivative is easily obtained from (37) and is given with

$$\frac{\partial \psi(x,t)}{\partial x} = A \frac{F}{V' g_2} \left(t + \mu_0 \rho_1^2 \int \frac{\sigma_{\|} g_1 V'}{F} \int \frac{F}{V' g_2} dxdx \right). \tag{40}$$

Second derivative of the poloidal flux is obtained in a straightforward manner as

$$\frac{\partial^2 \psi(x,t)}{\partial x^2} = A \frac{\partial}{\partial x}\left(\frac{F}{V' g_2} \right) t + A \mu_0 \rho_1^2 \left(\frac{\partial}{\partial x}\left(\frac{F}{V' g_2} \right) \int \frac{\sigma_{\|} g_1 V'}{F} \int \frac{F}{V' g_2} dxdx + \sigma_{\|} \frac{g_1}{g_2} \int \frac{F}{V' g_2} dx \right). \tag{41}$$

It is important to point out that this second derivative does not suffer from numerical instabilities.

V. COMPUTATIONAL EXAMPLES

Methods described in previous chapters are applied to an ITER hybrid scenario CRONOS simulation from [14] and obtained results are subsequently compared. It is worth emphasizing that in CRONOS the average current term is computed using cubic spline interpolation which is used for all derivatives with the default tension of the function. The edge value is constrained using AGSE since only fist derivative enters the formula. Diamagnetic function and geometrical coefficients are provided by the equilibrium code.

In particular, three time slices (905 s, 1000 s and 1095 s) from the late flat-top phase, where the current is almost fully diffused and thus all profiles tend to be stationary, are computed.

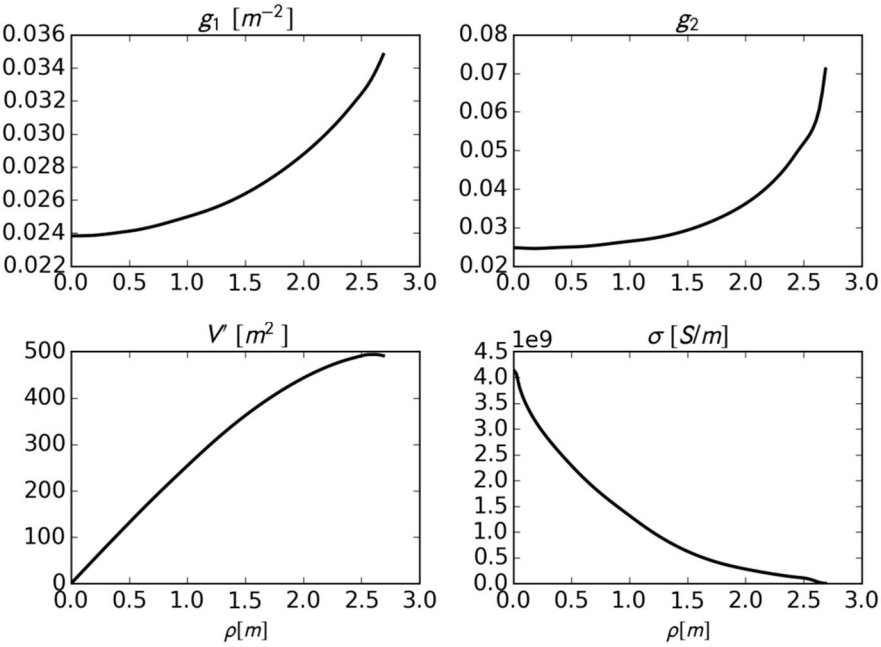

FIG. 2. Geometrical coefficients and conductivity from the CRONOS ITER hybrid mode simulation, times 905 s, 1000 s and 1095 s. The curves for all time slices tend to overlap.

A. Without non inductive current sources

As a first set of computational examples, a case without non inductive current sources (j_{ni}=0) is assumed. The results obtained with three proposed approaches (FEM – Linear, FEM – Hermite, Analytical) are compared. In Figure 3, a comparison of poloidal magnetic flux is shown in time instance t=905 s.

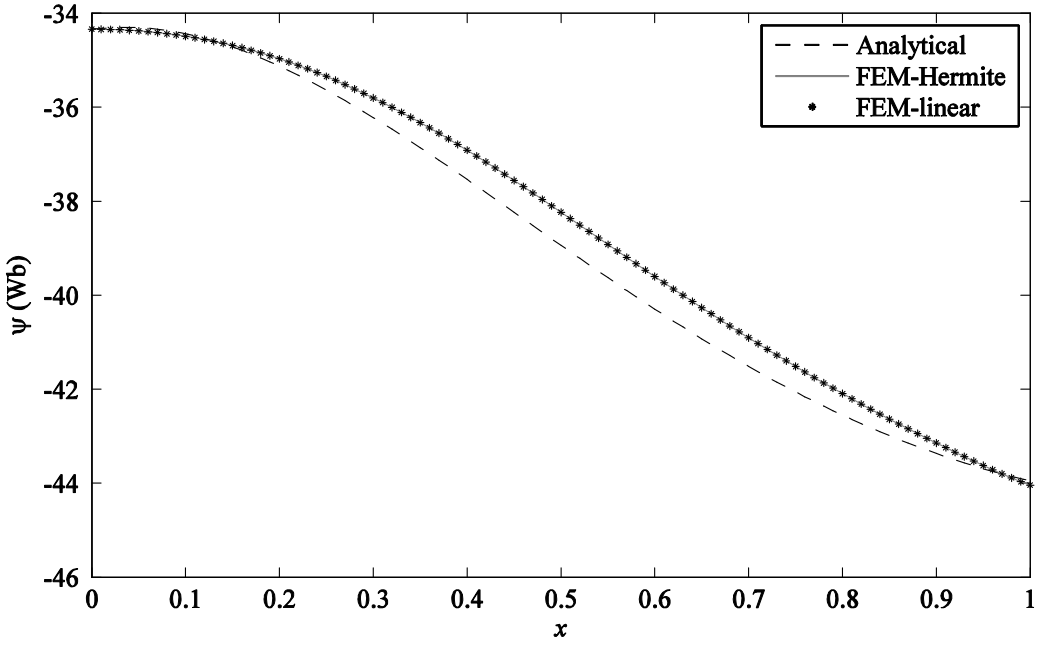

FIG. 3. Poloidal magnetic flux for t=905 s.

As it can be seen from the Fig. 3, results obtained with different basis functions (Linear and Hermite) agree perfectly. On the other hand, analytical approach differs in the middle of plasma. However, since maximum discrepancy of the results is less than 2%, overall agreement of the results is more than satisfactory considering the limitations of the analytical approach.

In Figures 4 and 5 the poloidal flux in time instances t=1000 s and 1095 s is shown with a comparison between Hermite and linear numerical approximation as well as analytical approach.

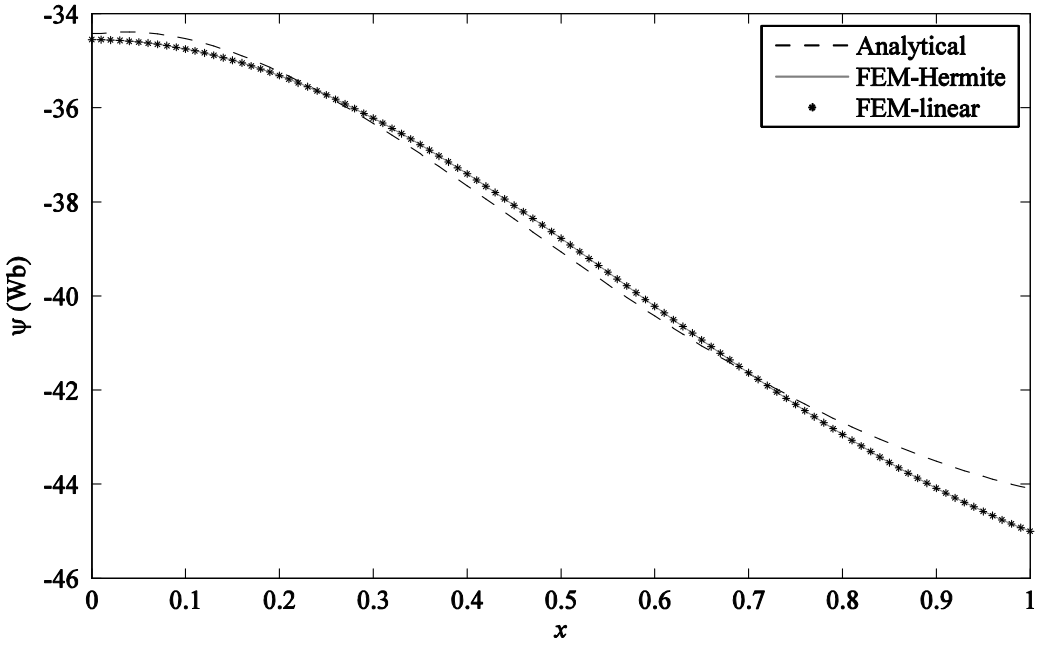

FIG. 4. Poloidal magnetic flux for t=1000 s.

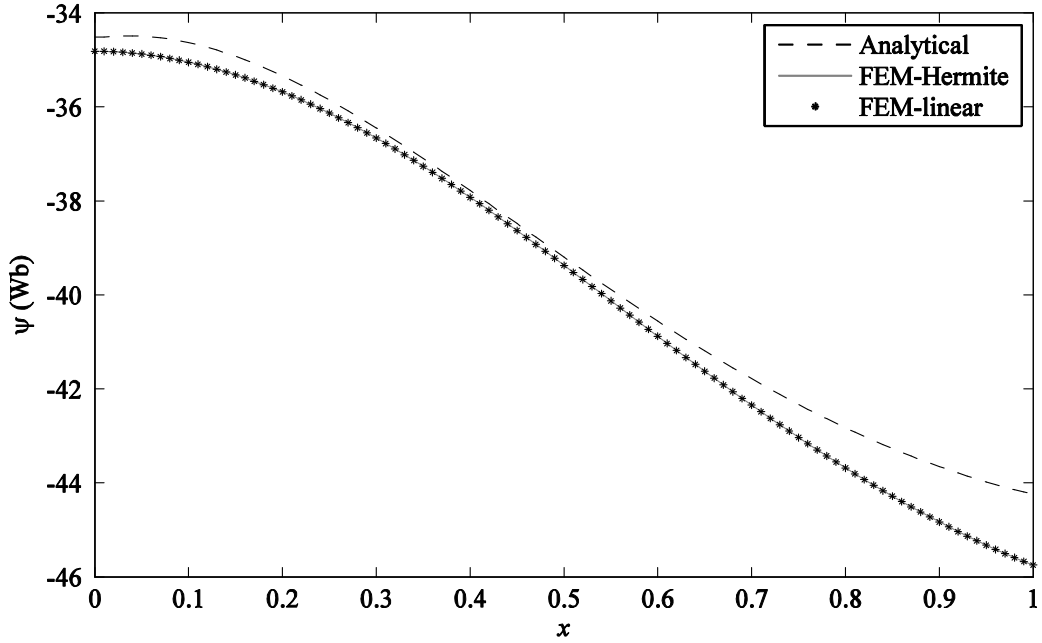

FIG. 5. Poloidal magnetic flux for t=1095 s.

The following set of results takes into account first and second derivative of poloidal flux calculated using Hermite, linear elements and analytical approach. In Fig. 6, the calculation of the first derivative for time instance t=1095 s is shown.

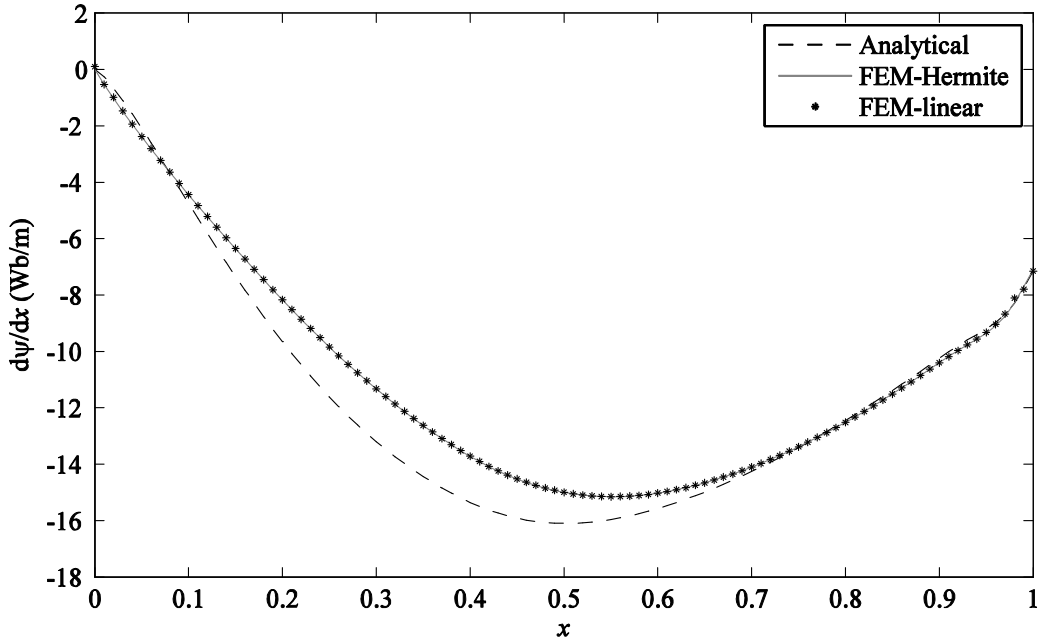

FIG. 6. First derivative of the poloidal magnetic flux for t=1095 s.

The results show good agreement at the edge of plasma, as well as overall agreement in the waveform, with some discrepancy shown in the middle. In Fig. 7 the second derivative of the

poloidal flux is shown for t=1095 s, calculated using numerical (linear and Hermite basis functions) and analytical approach.

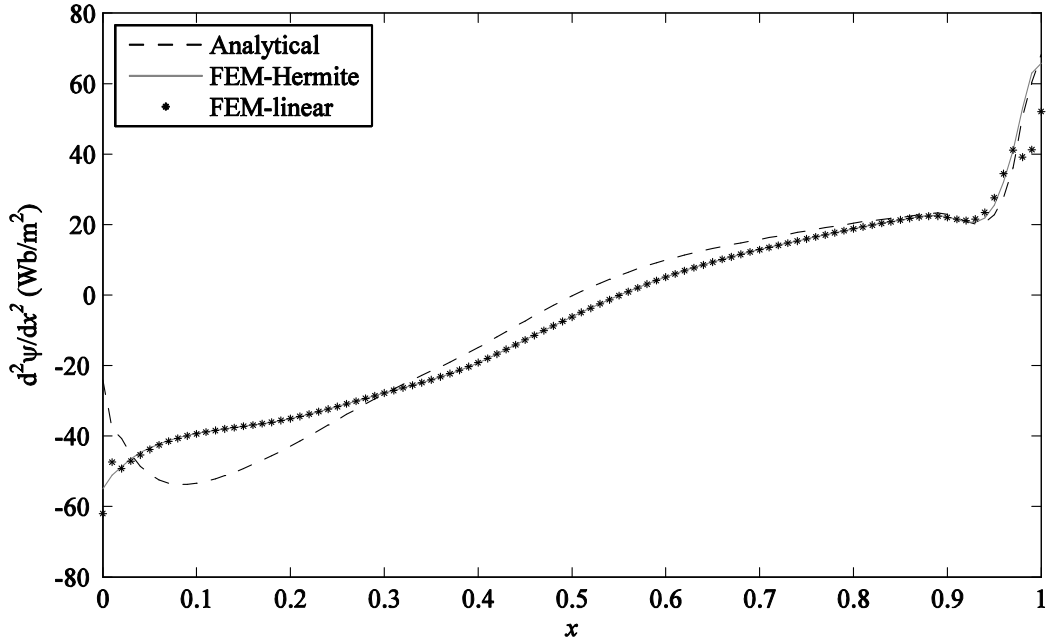

FIG. 7. Second derivative of the poloidal magnetic flux for t=1095 s.

It is shown that Hermite basis functions are better suited to calculate second derivative at the beginning of the domain, since they don't produce non-physical oscillations. It can be observed that analytical solution shows no oscillations and has generally good agreement with the numerical one.

B. With non-inductive current source

In this section, a case with the presence of non-inductive current sources is studied. The results obtained with the proposed numerical approaches (Linear and Hermite) and are compared with the results obtained via CRONOS calculations. Additional comparison with the results obtained with analytical approach is also given in order to compare it to the realistic case.

In Figure 8, a comparison of poloidal magnetic flux is shown for time instance t=905 s.

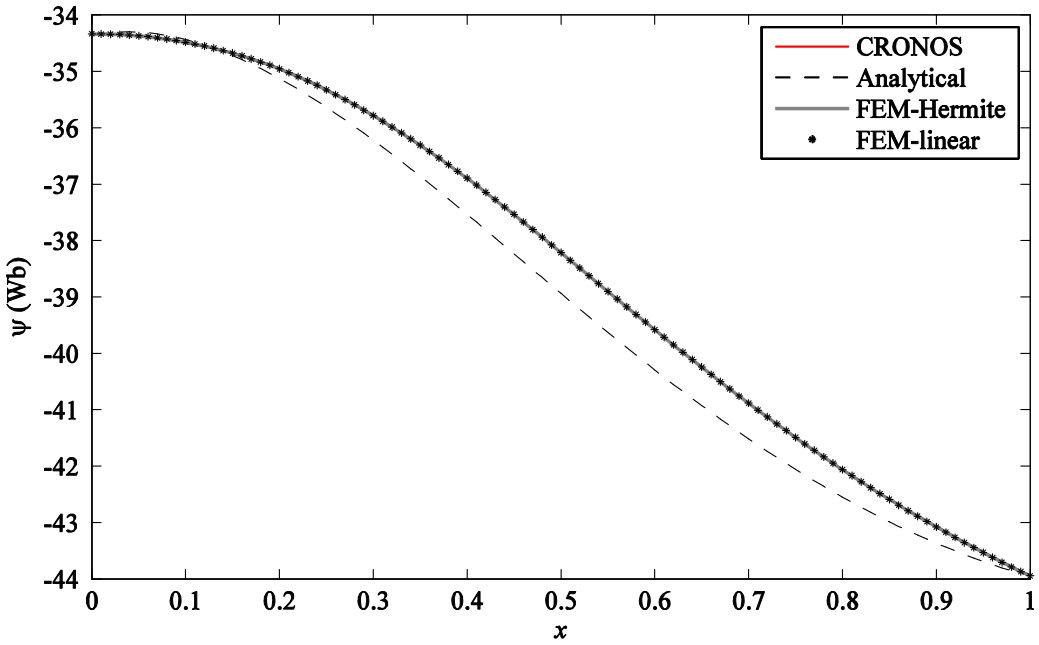

FIG. 8. Poloidal magnetic flux for t=905 s with non-inductive current sources.

As it can be seen from the Fig. 8, results obtained with numerical solution agree perfectly with the results from CRONOS calculations. The analytical approach shows similar behavior as in previous example.

In Figures 9 and 10 the poloidal flux for time instances t=1000 s and 1095 s is shown with a comparison between CRONOS, Hermite and linear numerical approximation as well as analytical approach.

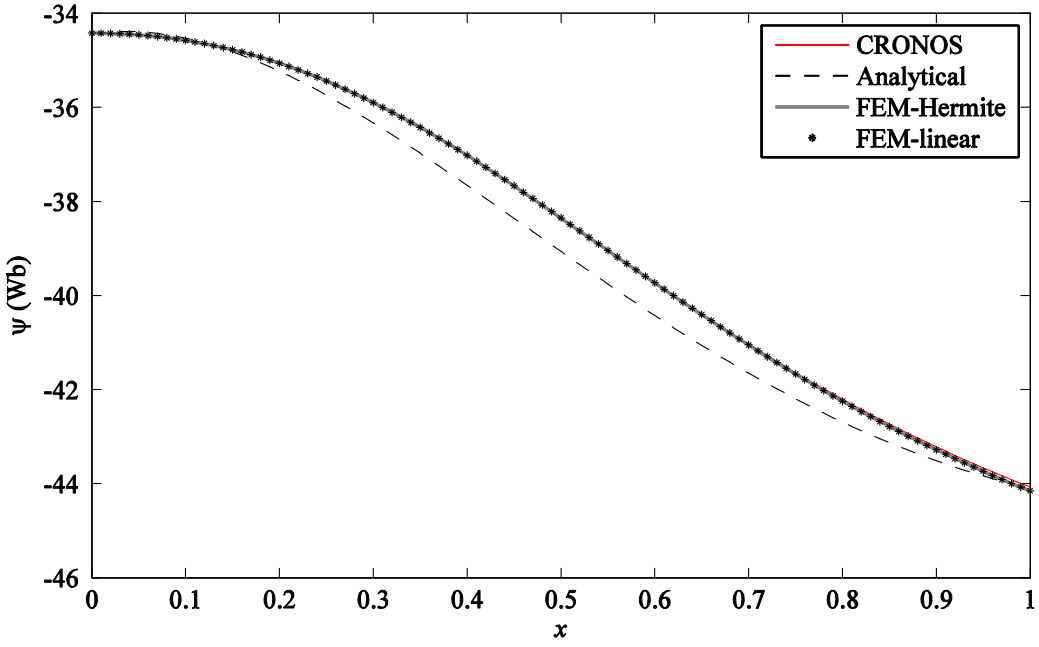

FIG. 9. Poloidal magnetic flux for t=1000 s with non-inductive current sources.

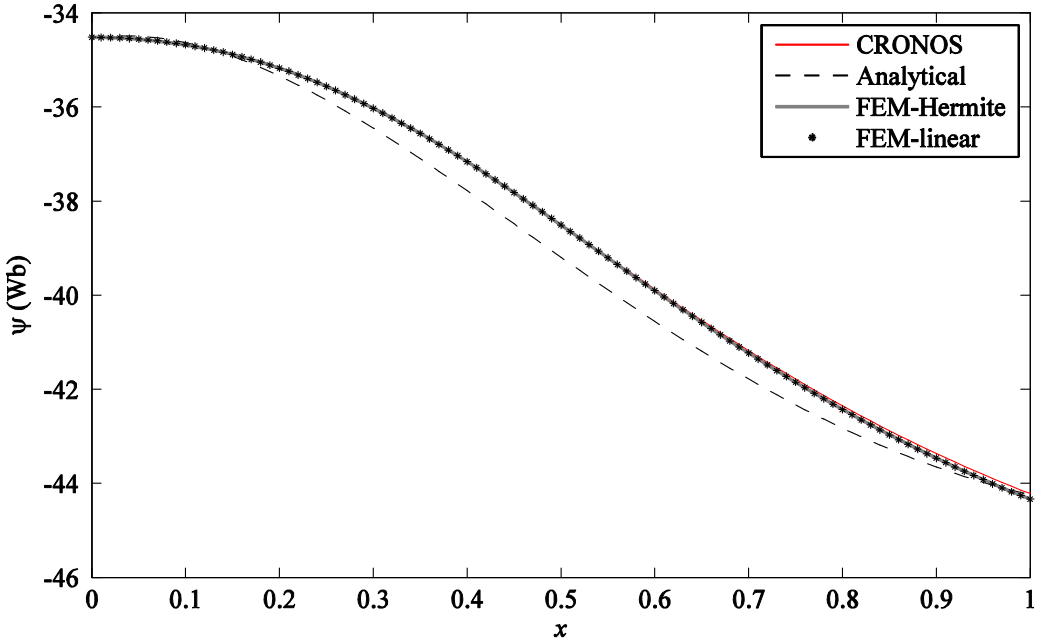

FIG. 10. Poloidal magnetic flux for t=1095 s with non-inductive current sources.

The following set of results takes into account first and second derivative of poloidal flux calculated using CRONOS, Hermite, linear elements and analytical approach. In Fig. 11, the calculation of the first derivative for time instance t=1095 s is shown.

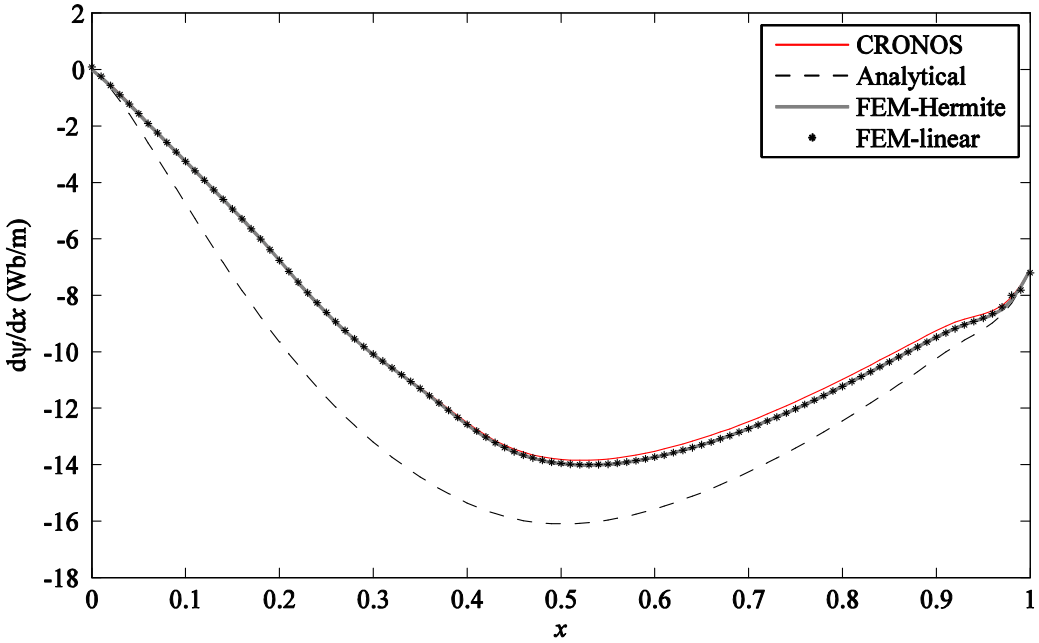

FIG. 11. First derivative of the poloidal magnetic flux for t=1095 s with non-inductive current sources.

The results show good agreement between results obtained with CRONOS and the numerical approach. Analytical results show the same discrepancy as in the previous case. In Fig. 12 the second derivative of the poloidal flux is shown for t=1095 s, calculated using CRONOS, numerical (linear and Hermite basis functions) and analytical approach.

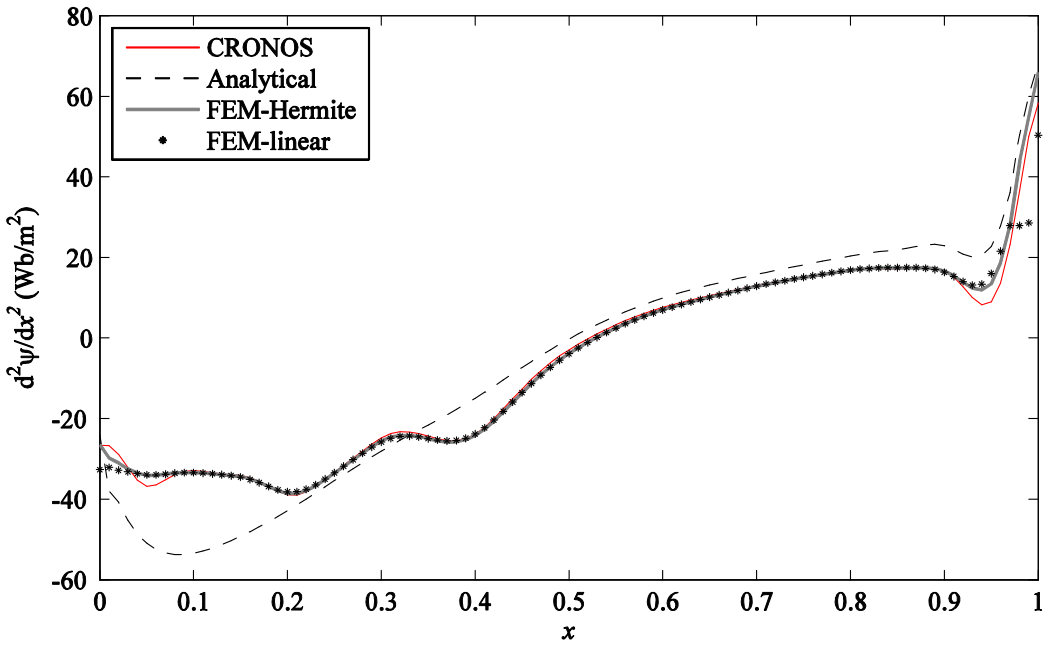

FIG. 12. Second derivative of the poloidal magnetic flux for t=1095 s with non-inductive current sources.

Again, it is shown that Hermite basis functions are better suited to calculate second derivative at the beginning of the domain, since they don't produce non-physical oscillations.

C. Average current

Average current is calculated using the data obtained for the first derivative of flux according to (7). Both cases (with and without non-inductive current sources) are taken into account and are shown in Figures 13. and 14. Similar to the results for the second derivative of flux, FEM solution using Hermite basis functions shows very good agreement with the results obtained with CRONOS. Analytical solution shows acceptable behavior for benchmarking purposes.

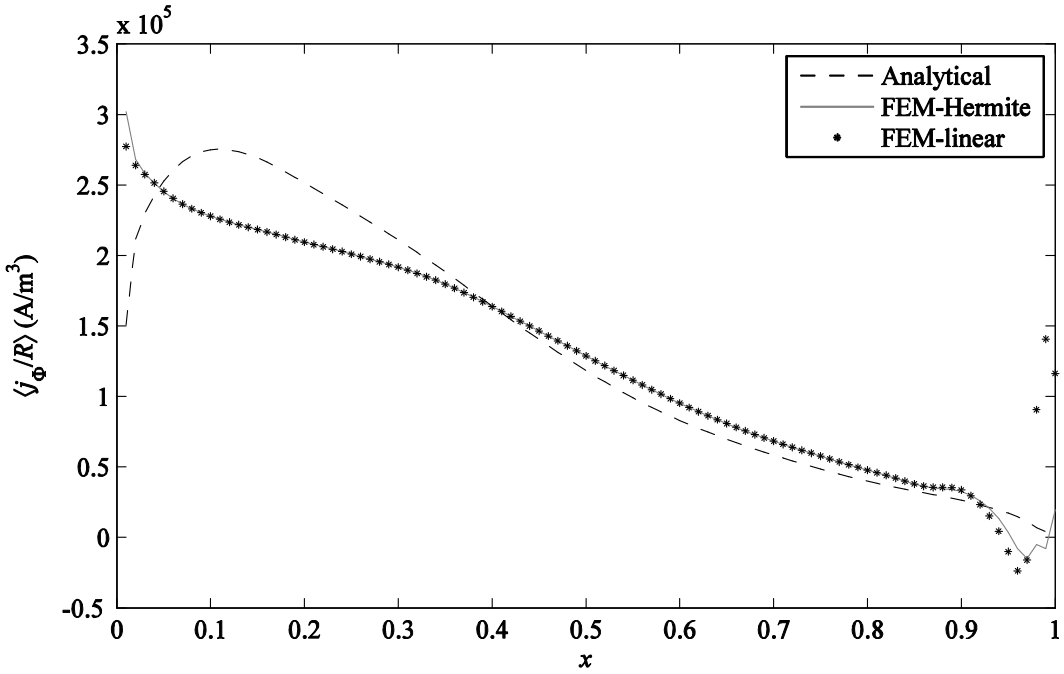

FIG. 13. Average current for t=1095 s without non-inductive current sources.

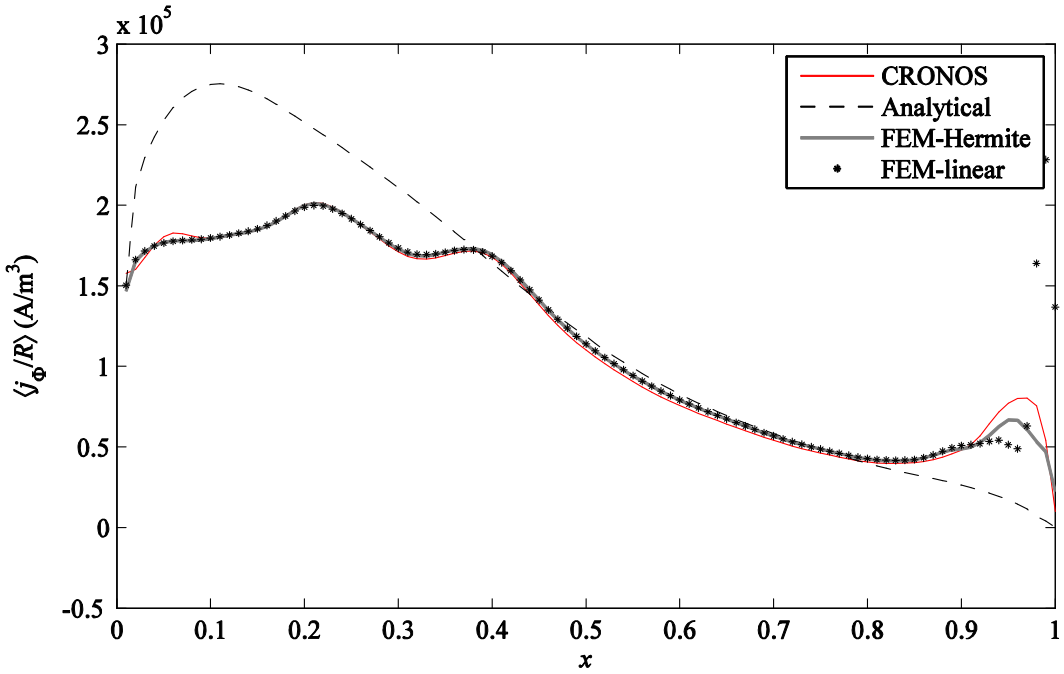

FIG. 14. Average current for t=1095 s with non-inductive current sources.

VI. CONCLUSION

The paper deals with two different approaches for the solution of the Current Diffusion Equation (CDE); Finite Element Method (FEM) and the analytical solution. The obtained

results are compared to the CRONOS tokamak transport suite calculations and the trade-off between different approaches has been carried out. The FEM solution is undertaken featuring the use of linear and Hermite type shape functions, respectively, while the analytical solution features the implementation of a specific procedure for the solution of space-time differential equations. The FEM solution shows excellent agreement with the results arising from CRONOS calculations, while providing stability inherent with the use of FEM scheme and Hermit basis functions, especially for the first and second derivative. The results obtained via analytical approach show rather satisfactory agreement with other methods, and therefore, due to its simplicity, makes it very suitable for benchmarking purposes. Also, it is important to emphasize that both numerical and analytical solutions for the derivative of flux agree in the edge region which is crucial for Grad-Shafranov Equation – Current Diffusion Equation (GSE-CDE) coupling.

ACKNOWLEDGEMENTS

This work has been carried out within the framework of the EUROfusion Consortium and has received funding from the Euratom research and training programme 2014-2018 under grant agreement No 633053. The views and opinions expressed herein do not necessarily reflect those of the European Commission.
Work performed under EUROfusion WP CD, supported by the EUROfusion-IM Team (see http://www.euro-fusionscipub.org/eu-im).
The work of J. Urban was funded by project MSMT LM2011021.

REFERENCES

[1] G. Falchetto et al., "The European Integrated Tokamak Modelling (ITM) effort: achievements and first physics results," *Nuclear Fusion,* vol. 54, p. 043018, 2014.

[2] V. S. Mukhovatov and V. D. Shafranov, "Plasma Equilibrium in a Tokamak," *Nuclear Fusion,* vol. 11, pp. 605-633, 1971.

[3] F. Hinton and R. Hazeltine, "Theory of plasma transport in toroidal confinement systems," *Reviews of Modern Physics,* vol. 48, pp. 239-308, 1976.

[4] J. Blum and J. Lefoll, "Plasma Equilibrium Evolution at the Resistive Diffusion Timescale," *Computer Physics Reports,* vol. 1, no. 7-8, pp. 465-494, 1984.

[5] H. Grad, P. N. Hu and D. C. Stevens, "Adiabatic Evolution of Plasma Equilibrium,"

Proceedings of the National Academy of Sciences of the United States of America, vol. 72, pp. 3789-3793, 1975.

[6] H. Grad and J. Hogan, "Classical Diffusion in a Tokomak," *Physical Review Letters,* vol. 24, pp. 1337-1340, 1970.

[7] J. F. Artaud et al., "The CRONOS suite for integrated tokamak modelling," *Nuclear Fusion,* vol. 50, pp. 1-25, 2010.

[8] R. R. Khayrutdinov and V. E. Lukash, "Studies of plasma equilibrium and transport in a tokamak fusion device with the inverse-variable technique," *Journal of Computational Physics,* vol. 109, no. 2, pp. 193-201, 1993.

[9] E. Fable et al., "A stable scheme for computation of coupled transport and equilibrium equations in tokamaks," *Nuclear Fusion,* vol. 53, no. 3, 2013.

[10] D. Coster, V. Basiuk, G. Pereverzev, D. Kalupin, R. Zagorski, R. Stankiewicz, P. Huynh and F. Imbeaux, "The European Transport Solver," *IEEE Transactions on Plasma Science,* vol. 38, no. 9, pp. 2085 - 2092, 2010.

[11] F. Felici et al., "Real-time physics-model-based simulation of the current density profile in tokamak plasmas," *Nuclear Fusion,* vol. 51, no. 8, pp. 1-19, 2011.

[12] P. Holoborodko, "Smooth Noise Robust Differentiators," 2008. [Online]. Available: http://www.holoborodko.com/pavel/numerical-methods/numerical-derivative/smooth-low-noise-differentiators/. [Accessed 30 11 2015].

[13] A. D. Polyanin, Handbook of linear partial differential equations for engineers and scientists, Boca Raton, London, New York, Washington, D.C.: Chapman & Hall/CRC, 2002.

[14] V. Parail et al., "Self-consistent simulation of plasma scenarios for ITER using a combination of 1.5D transport codes and free-boundary equilibrium codes," *Nuclear Fusion,* vol. 53, no. 11, p. 113002, 2013.